CARBON 85 (2015) 89–98

Available at www.sciencedirect.com

ScienceDirect

journal homepage: www.elsevier.com/locate/carbon

Nanopatterning on highly oriented pyrolytic graphite surfaces promoted by cobalt oxides

D. Díaz-Fernández [a], J. Méndez [b], A. del Campo [c], R.J.O. Mossanek [d], M. Abbate [d], M.A. Rodríguez [c], G. Domínguez-Cañizares [a], O. Bomatí-Miguel [a], A. Gutiérrez [a], L. Soriano [a,*]

[a] Departamento de Física Aplicada and Instituto de Ciencia de Materiales Nicolás Cabrera, Universidad Autónoma de Madrid, Cantoblanco, E-28049 Madrid, Spain

[b] ESISNA Group, Instituto de Ciencia de Materiales de Madrid, ICMM-CSIC, Cantoblanco, E-28049 Madrid, Spain

[c] Instituto de Cerámica y Vidrio, ICV-CSIC, C/Kelsen, 5, Cantoblanco, E-28049 Madrid, Spain

[d] Departamento de Física, Universidade Federal do Paraná, Caixa Postal 19044, 81531-990 Curitiba, PR, Brazil

ARTICLE INFO

Article history:
Received 20 September 2014
Accepted 4 December 2014
Available online 20 December 2014

ABSTRACT

In this work we present a method to produce nanopatterning on graphite surfaces via carbon gasification reaction, with oxygen as reactant gas, catalyzed by cobalt oxides (CoO) instead of metallic cobalt nanoparticles as most usual methods. This reaction is produced at 400 °C, temperature which is much lower than that used in conventional methods. The chemical analysis of the cobalt species have been performed with X-ray photoemission and X-ray absorption spectroscopies, which are supported by theoretical cluster model and multiplet calculations of the spectra. The changes in the morphology of the surfaces after each process have been followed by atomic force microscopy. The defects produced after the gas reaction on the graphite surface have also been analyzed by combining atomic force microscopy and confocal micro-Raman spectroscopy. The presence of oxygen in the initial CoO wetting-layer has been identified as responsible of the weakening of the graphite bonds at the surface.

1. Introduction

The main purpose of this paper is to study a method of nanopatterning in graphite via carbon gasification at 400 °C starting with cobalt oxide as catalyst material instead of metallic cobalt nanoparticles, like most usual methods performed at higher temperatures do. Since the discovery of the unique physical and chemical properties of graphene, the possibility of fabricating nanostructures by patterning on graphene and graphite surfaces has become a hot research topic due to the multiple applications these materials find in many technological fields [1]. Different from most of the patterning techniques, including lithography [2], plasma etching [3] and electro catalysis using scanning probe microscopes [4,5], carbon gasification catalyzed by metallic nanoparticles in controlled atmosphere at high temperatures has demonstrated to be one of the most efficient methods as cutting tool for graphene [6]. Carbon gasification reactions have been studied using a large variety of metallic nanoparticles and reactant gases such as steam, molecular oxygen, carbon dioxide and hydrogen. For instance, Ci et al. [6] reported the use of Ni nanoparticles and hydrogen for the fabrication of

* Corresponding author.
E-mail address: l.soriano@uam.es (L. Soriano).
http://dx.doi.org/10.1016/j.carbon.2014.12.049
0008-6223/

single etch patterns in highly oriented pyrolytic graphite (HOPG) at temperatures ranging from 750 °C to 1100 °C; Severin et al. [7] have used silver nanoparticles and molecular oxygen to produce channelling in graphene at 650 °C; Konishi et al. [8] used Co nanoparticles heated under a gas mixture stream of high purity H_2 (10%) + N_2 (90%) gas at 700 °C; Datta et al. [9] have reported the Crystallographic Etching of graphene using Fe nanoparticles in H_2 and Ar_2 atmosphere at 900 °C. Moreover, by taking advantage of the ferromagnetic behavior of the cobalt nanoparticles, Bulut et al. reported a writing method on HOPG surfaces steered by magnetic fields at about 550 °C in air [10]. All these reported methods for channelling formation by carbon gasification are efficient at relatively high temperatures (>600 °C). In general, gasification reactions between carbon and the reactant gas are produced at the carbon-catalyst particles interface (solid/solid/gas reaction), resulting in pitting and deep channelling of the carbon surface with the movement of the catalyst particle along the basal plane [11]. The oxidation of graphite using transition metal oxides as catalysts has also been reported [12] concluding that only those transition metals with two oxidation states are capable of such oxidation. More recently, creation of defects on multi-walled carbon nanotubes by CoO has also been reported [13–15].

The study of the early stages of growth of cobalt oxides by reactive cobalt evaporation in oxygen atmosphere ($PO_2 = 2 \times 10^{-5}$ mbar) on HOPG has already been studied by us [16]. It was concluded that CoO grows following a Stranski–Krastanov way of growth, i.e. the formation of a wetting layer followed by the growth of islands. At the early stages of growth, strong diffusion of the adsorbates towards the HOPG steps and the formation of a CoO wetting layer 4 Å thick (2 monolayers) on the HOPG surface have been observed, being CoO (Co^{2+}) the only species formed. Further evaporation produces the formation of CoO islands on the above wetting layer up to coverages of about 30 equivalent monolayers (Eq-ML) where coalescence is produced. In contrast, further coverages lead to the formation of the spinel Co_3O_4 oxide ($Co^{2+,3+}$).

The chemical analysis has been performed by means of X-ray photoemission (XPS) and X-ray absorption (XAS) spectroscopies. Both techniques are well suited for the chemical characterization of the species involved in the experiments, especially the oxidation state of Co. The main difference of these techniques is their different probing depth, being 15 Å [17] for XPS and about 40 Å [18] for XAS. The experimental spectra are supported by theoretical cluster model calculations for the XPS spectra and atomic multiplet calculations, including charge transfer and crystal field effects, for the XAS spectra. The channelling formation has been observed and analyzed by means of Atomic Force Microscopy (AFM). In addition, the defects produced on the graphite surface under this reaction have been studied by means of combined Atomic Force Microscopy (AFM) and confocal micro-Raman spectroscopy.

Although different methods to produce nanopatterning on HOPG surfaces using metallic and oxide particles have been reported, the mechanisms involved in these methods are not completely understood yet. In this work we present not only a more efficient patterning method on graphite at lower temperatures (400 °C) than those using metallic nanoparticles reported in the literature, but also a detailed analysis of both, catalyst and substrate, giving relevant information on the mechanism involved in such reaction. Our method uses a cobalt oxide (CoO) ultra-thin layer grown on the HOPG substrate as starting catalyst material (see below), and molecular oxygen as reactant gas. It is demonstrated that at this temperature this method is more efficient to produce nanochannelling in graphite using CoO oxide as catalyst than using metallic cobalt.

2. Experimental

The experiments related to this study have been performed in two different ultra-high-vacuum (UHV) chambers, one attached to the analysis chamber of the XPS spectrometer in our laboratory and the other located at the Suricat UHV system attached at the PM4 beamline at the synchrotron BESSY II (Berlin). In both cases we started the experiments with the growth of an ultra-thin CoO layer of 2 equivalent monolayers thickness (ML) on an HOPG graphite substrate by reactive thermal evaporation of metallic cobalt in a molecular oxygen atmosphere ($PO_2 = 2 \times 10^{-5}$ mbar), with 1×10^{-9} mbar as base pressure of the chamber and maintaining the substrates at room temperature. The evaporation rate was maintained constant and very low in order to control the low coverage of cobalt oxides on the substrate (0.25 Eq.-ML/min, taking 1 Eq.-ML ≈ 2 Å). The HOPG substrate (Broker, ZYB grade) was first cleaved using a scotch tape and immediately introduced under vacuum conditions (1×10^{-8} mbar) and then heated up to 400 °C in order to remove possible contamination. Once CoO was grown, it was submitted to a re-oxidation process, basically consisting of exposure to oxygen atmosphere ($PO_2 = 2 \times 10^{-3}$ mbar) and thermal annealing at 400 °C for 1 h. However, in order to distinguish the effect of both, oxygen exposure and thermal annealing, the re-oxidation process was performed in two different ways: for the first process (in the following labeled as Reox-P1), the oxygen exposure was delayed until the substrate temperature reached 400 °C in ultra-high vacuum conditions, approximately in 10 min. In the second process (Reox-P2) the oxygen exposure was started with the sample at room temperature, then reaching 400 °C while it was exposed to the oxygen atmosphere. Also a 3 ML's thick overlayer of metallic cobalt was grown under UHV conditions in order to compare its behavior when submitted to the re-oxidation process Reox-P1.

The X-ray photoemission spectra (XPS) were taken with a CLAM-4 MCD hemispherical analyser from Thermo Fisher Scientific using Mg K_α radiation. The pass energy of the analyser was set to 20 eV, giving a resolution of about 0.9 eV. The energy scale was calibrated by adjusting the C1s peak of the HOPG substrate at 284.3 eV [19]. The X-ray absorption (XAS) and photoemission (PES) spectra were obtained at the PM4 beamline in BESSY II which is equipped with a plane-grating monochromator. The XAS spectra were collected in the total electron yield mode by measuring the drain current

from the sample and normalized to the I_0 current measured from a gold reference sample. The optical arrangement of this monochromator was set to optimize both photon flux and energy resolution, in order to obtain an acceptable signal from the very small amount of material deposited. The estimated overall resolution was better than 100 meV at 530 eV. Also surface sensitive photoemission spectra (PES) of the C 1s core-level were taken by using a hemispherical electron energy analyzer (Scienta SES 100) with 120 meV energy resolution at 20 eV pass energy. The AFM images were obtained with a Nanotec AFM microscope in the non-contact dynamic (tapping) mode, using modified tips with Au nanoparticles [20] and were processed and analyzed with the WSxM software [21]. Raman images were obtained using a confocal Raman microscope coupled with and atomic force microscope (AFM) instrument (Witec ALPHA 300RA) with laser excitation at 532 nm and a 100× objective lens (NA = 0.9). The incident laser power was 5 mW. The optical diffraction resolution of the confocal microscope was limited to about ~200 nm laterally and ~500 nm vertically. Raman spectral resolution of the system was down to 0.02 cm^{-1}. The samples were mounted in a piezo-driven scan platform having 4 nm lateral and 0.5 nm vertical positioning accuracy. The piezoelectric scanning table allows three-dimensional displacements in steps of 3 nm (0.3 nm in vertical direction), giving a very high spatial resolution for both the AFM and confocal Raman microscopy. The microscope base was also equipped with an active vibration isolation system, active 0.7–1000 Hz. The system allows studying the same area of the sample by selecting the adequate objective of the microscope. Collected spectra were analyzed by using Witec Control Plus software.

3. Results and discussion

3.1. The oxidation state of cobalt

Fig. 1 shows the Co 2p core-level XPS and XAS spectra of each step of the processes described in the experimental section. It is known that the oxidation state of cobalt catalysts surfaces may vary distinctively in the presence of oxygen as reactant gas [22], therefore the determination of the Co species involved in each of those processes is important to a better understanding of the mechanisms involved in the studied reaction. All the spectra present two main regions, the Co $2p_{3/2}$ and Co $2p_{1/2}$ levels, due to spin–orbit coupling. The Co $2p_{3/2}$ XPS spectrum of the initial cobalt oxide wetting layer (2 Eq.-ML) grown on HOPG, labeled "as grown", consists of a main peak located at about 781 eV and a satellite at 786 eV, whereas the XAS spectrum exhibits a series of structures attributed to multiplet effects. These spectra are fairly well reproduced by the calculations, when considering a high spin configuration of Co^{2+} ions in octahedral symmetry with a crystal field (10 Dq) of 0.5 eV. This is somewhat smaller than the usual value of 10 Dq for bulk CoO oxide, which is about 1.05 eV [23]. The reduced crystal field, in this case, is consistent with a decrease of coordination of the cobalt atoms in the CoO over-layer, and also coherent with its growth by thermal evaporation at room temperature and with the bi-dimensional character of the CoO wetting layer observed in Ref. [16].

The next step consisted of annealing the sample at 400 °C for 30 min in UHV, labeled as "heated". The XPS and XAS spectra change, being much narrower than the previous ones, where the satellite in the XPS spectrum (Fig. 1a), as well as the

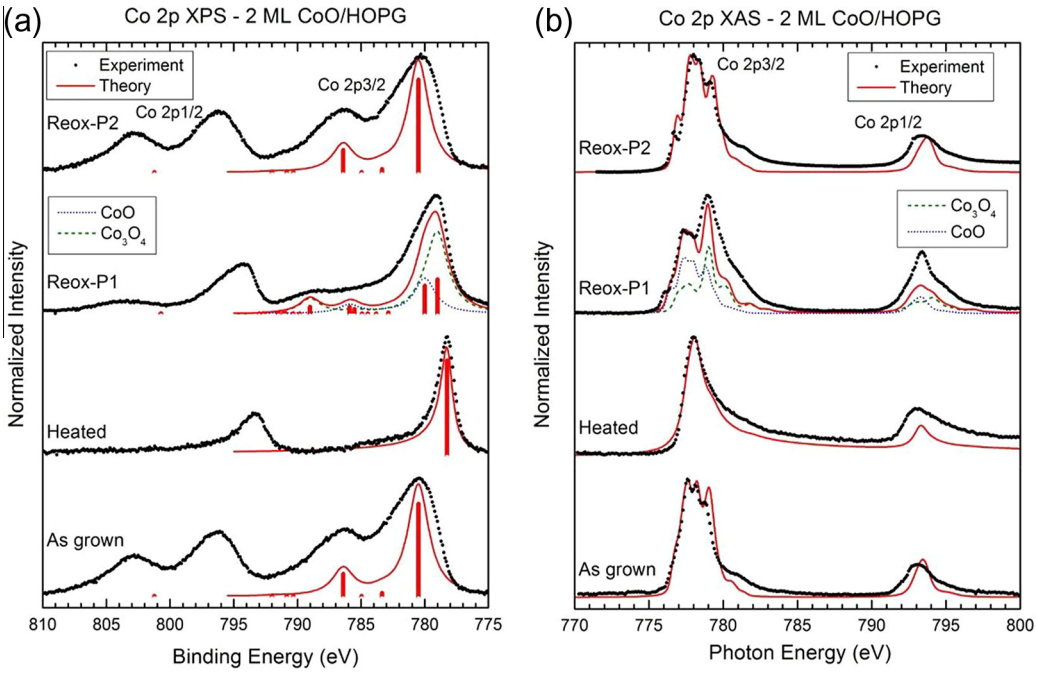

Fig. 1 – Experimental (dots) and theoretical (lines) spectra of the Co 2p XPS spectra (a) and XAS spectra (b) of the initial CoO ultra-thin layer as grown (bottom spectra) and submitted to each process (as labeled). For explanation see text. (A color version of this figure can be viewed online.)

multiplet structure in the XAS spectrum (Fig. 1b) vanish. These spectra are now related to metallic Co, for which the calculations are again in good agreement. Therefore, the results indicate that the first step of the re-oxidation process P1 reduces the initial CoO overlayer to metallic cobalt previously to the oxygen exposure. This result is consistent with the reducing character of the graphite substrate.

After the complete re-oxidation process, labeled "Reox-P1", the XPS and XAS spectra differ from those observed before. The main difference in the XPS spectrum is that the main peak is slightly shifted by 1 eV towards lower binding energies, and the satellite almost disappears, giving rise to two small satellites located at 786 eV and 789 eV. At first, this could indicate that the sample is now in the spinel Co_3O_4 phase, i.e. a combination of Co^{2+} in tetrahedral and Co^{3+} in octahedral symmetry. Nevertheless, the XAS spectrum shows again different multiplet structures, which cannot be reproduced solely with spinel structure. The lower energy structures (777–778 eV) are similar to those observed in the "as grown" sample, suggesting that this spectrum corresponds to a mixture of CoO and Co_3O_4 oxides. In fact, both experimental spectra are well reproduced by the calculations of a mixture of around 30% of Co^{2+} in octahedral symmetry (dotted blue curve) and about 70% of spinel Co_3O_4 (dashed green curve). These results show that after the complete re-oxidation process P1, the reduced Co particles have been oxidized to Co_3O_4, with a remaining small fraction of CoO. On the other hand, when the initial CoO layer is submitted to the re-oxidation process P2, labeled "Reox-P2", the XPS spectrum is identical to that of the "as grown" sample, and the XAS spectrum differs from it in the appearance of a new peak at threshold around 776 eV. The calculations again correspond to a high spin configuration of Co^{2+} ions in octahedral symmetry, but now with a crystal field (10 Dq) of 0.9 eV. The larger crystal field in this case is consistent with the formation of a more ordered and better coordinated CoO layer after Reox-P2 process.

By summarizing the chemical analysis results, the Reox-P1 process reduces the initial CoO layer to metallic cobalt during the first step (heating in UHV) and then oxidizes the cobalt atoms located at the near-surface region to the spinel Co_3O_4 oxide upon oxygen exposure at 400 °C. In contrast, the Reox-P2 is not able to reduce the initial CoO layer neither to oxidize to Co_3O_4 maintaining the original oxidation state Co^{2+}. These results are completely consistent with the Hellingham diagrams depicted in Fig. S1 of the Supplementary information, where the free energy for the formation of CoO is much lower than for the formation of the spinel Co_3O_4 oxide.

3.2. *The channelling formation as observed by AFM*

We show in Fig. 2 the AFM images of the initial 2 ML of CoO on HOPG sample as grown and submitted to the different processes as labeled. The image corresponding to the as grown sample (Fig. 2a) consists of small dendritic CoO islands grown on the CoO wetting layer previously formed on the HOPG substrate. More details on the way of growth of CoO/HOPG can be found elsewhere [16]. We have to note that at this stage of growth, the HOPG surface is not completely covered by the CoO wetting layer thus, averaging the material deposited at the steps, the total equivalent coverage is 2 ML (see Ref. [16]). Fig. 2b corresponds to the same sample submitted to thermal annealing at 400 °C for 30 min in UHV conditions, i.e. the first step of process Reox-P1. According to the results of the previous section, the reduction of the initial CoO layer leads to the formation of metallic Co particles distributed through the HOPG surface. It is also observed the presence of blurred short lines following preferential directions forming angles of 60° and 120° with respect to each other. Similar preferential lines on HOPG and graphene had already been observed during the catalyzed hydrogenation of graphene at temperatures higher than 600 °C with Ni, Co, Fe nanoparticles, producing etching of the graphene surface along the crystallographic axes [6,8,9]. Fig. 2c shows the image of the as grown CoO layer after the whole Reox-P1 process. The image clearly shows the presence of multiple nano-channels with trajectories randomly distributed along the HOPG surface. The presence of small Co_3O_4 islands at the end of the channels suggests that these particles have moved randomly throughout the HOPG surface activated by temperature and react with the carbon atoms via gasification leading to the erosion of the surface and producing nano-channels. The width of the channels observed in the topographic images is determined by the lateral size of the Co nanoparticle whereas their depth is always a multiple of 3.35 Å (see Table 1), i.e. the distance between graphite planes [24]. These results suggest that carbon gasification reaction has been produced upon

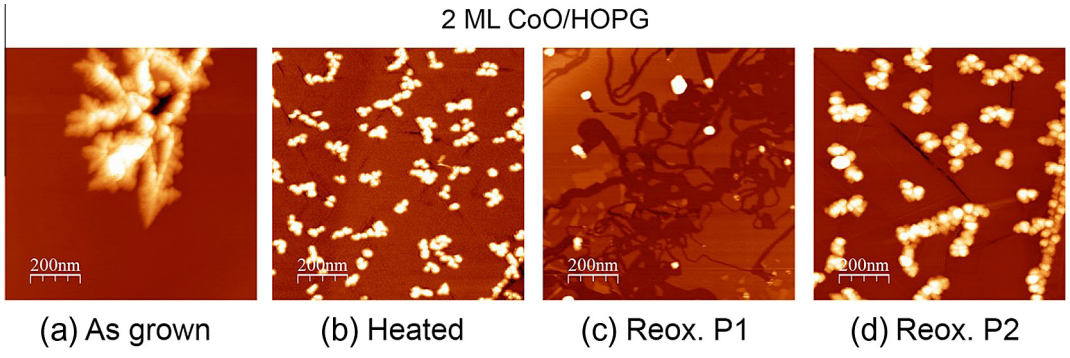

Fig. 2 – 1 × 1 μm² AFM images of the initial CoO ultra-thin layer as grown and submitted to each process (as labeled). (A color version of this figure can be viewed online.)

Table 1 – Averaged values of the nano-channels depth as observed in the AFM images.

Channel-depth (nm)	Number of planes (1 plane = 0.335 nm [23])
0.34 ± 0.02	1.02 ± 0.01
0.68 ± 0.04	2.06 ± 0.03
1.01 ± 0.09	3.03 ± 0.03

the Reox-P1 process. Residual Gas Analysis performed with a mass spectrometer indicates the production of CO when the oxygen exposure was initiated as observed in Fig. 3c. On the other hand, Fig. 3a and b show the AFM image taken in topographic and phase mode respectively from a devastated area of the graphite surface. As the information given by the AFM images taken in phase mode is related to the viscoelasticity of the probed material [25], it is inferred that the material of the nano-channel is also graphite, confirming the catalytic reaction of carbon gasification. Finally, Fig. 2d shows the result of the re-oxidation process P2 applied to the initial CoO layer. In this case no nano-channels are produced as in the re-oxidation process P1, however preferential lines following the crystallographic edges are clearly observed.

According to the AFM results the nano-channels are only produced when the initial CoO layer is submitted to complete Reox-P1 process, i.e. heating of the substrate up to 400 °C and posterior oxygen exposure at a pressure of 2×10^{-3} mbar. In contrast, when the re-oxidation process is performed by heating the initial CoO layer under the same oxygen environment (Reox-P2), no formation of nano-channels is observed. This result is not surprising as the intermediate state of the Reox-P1 process gives metallic Co particles which are known to produce similar channelling formation at higher temperatures [8].

3.3. *Reduced Co particles versus freshly evaporated Co particles*

In order to compare the above results, we have prepared a sample consisting of 3 Eq.-ML of freshly evaporated Co nanoparticles which have been submitted to Reox-P1. Fig. 4 shows the AFM images of the metallic Co nanoparticles as reduced from the initial CoO layer upon heating at 400 °C (Fig. 4a) and the Co nanoparticles formed by evaporation of metallic cobalt in UHV conditions (Fig. 4c). Two main differences of these Co nanoparticles are observed: firstly, the nanoparticles coming from the reduction of the initial CoO layer are smaller in size (25–50 nm) than those from the cobalt evaporation (50–100 nm). Secondly, the density of Co nanoparticles per unit area resulted from the evaporation is larger than that of the nanoparticles obtained upon reduction of the initial CoO layer. This latter difference is obviously due to the larger coverage of the initial evaporated nanoparticles than that of the initial CoO layer. But the main differences are observed in the images of those Co particles after the Reox-P1 process shown in Fig. 4b and d. Clearly, the nanoparticles formed upon reduction of the initial CoO layer efficiently produce nano-channelling, whereas the Co nanoparticles directly evaporated do not. Although it is known that metallic Co nanoparticles are able to promote carbon gasification and consequently nano-channelling of the HOPG surface at temperatures higher than 600 °C [8], it seems that at 400 °C they are not able to form nano-channels. At these high temperatures, one proposed mechanism is the possible formation of carbide-like at the interface. However at 400 °C we have observed an efficient way to create channelling starting with CoO instead of metallic Co nanoparticles which suggests that the role of the presence of oxygen seems to be relevant in this catalytic process. This is also supported, as shown in Fig. 5, by the final oxidation state of the evaporated cobalt

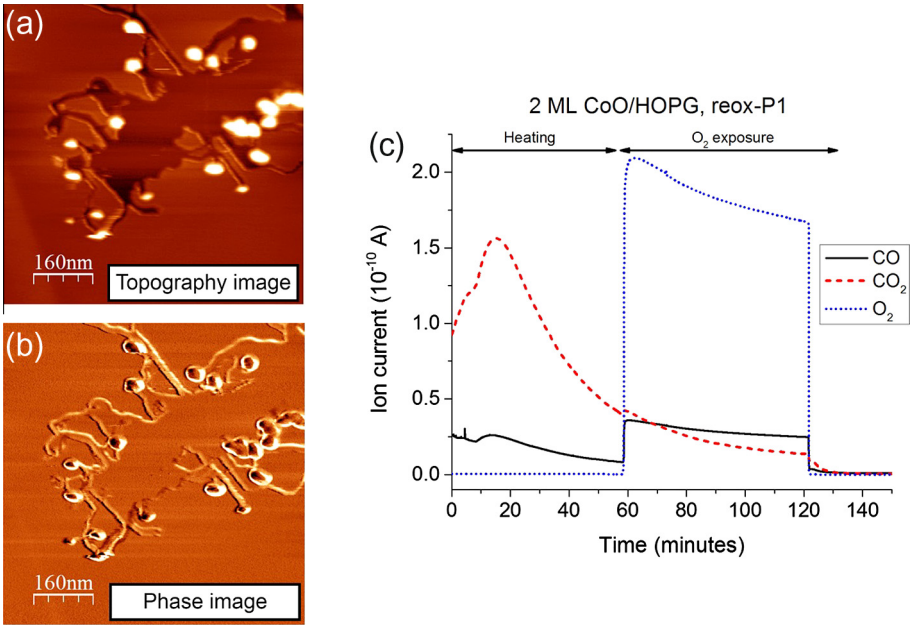

Fig. 3 – 800 × 800 nm² AFM images of the initial CoO layer submitted to the Reox-P1 process (a) taken in topographic mode and (b) phase mode. (c) Residual gas analysis (RGA) recorded during the Reox-P1 process of the initial CoO layer. (A color version of this figure can be viewed online.)

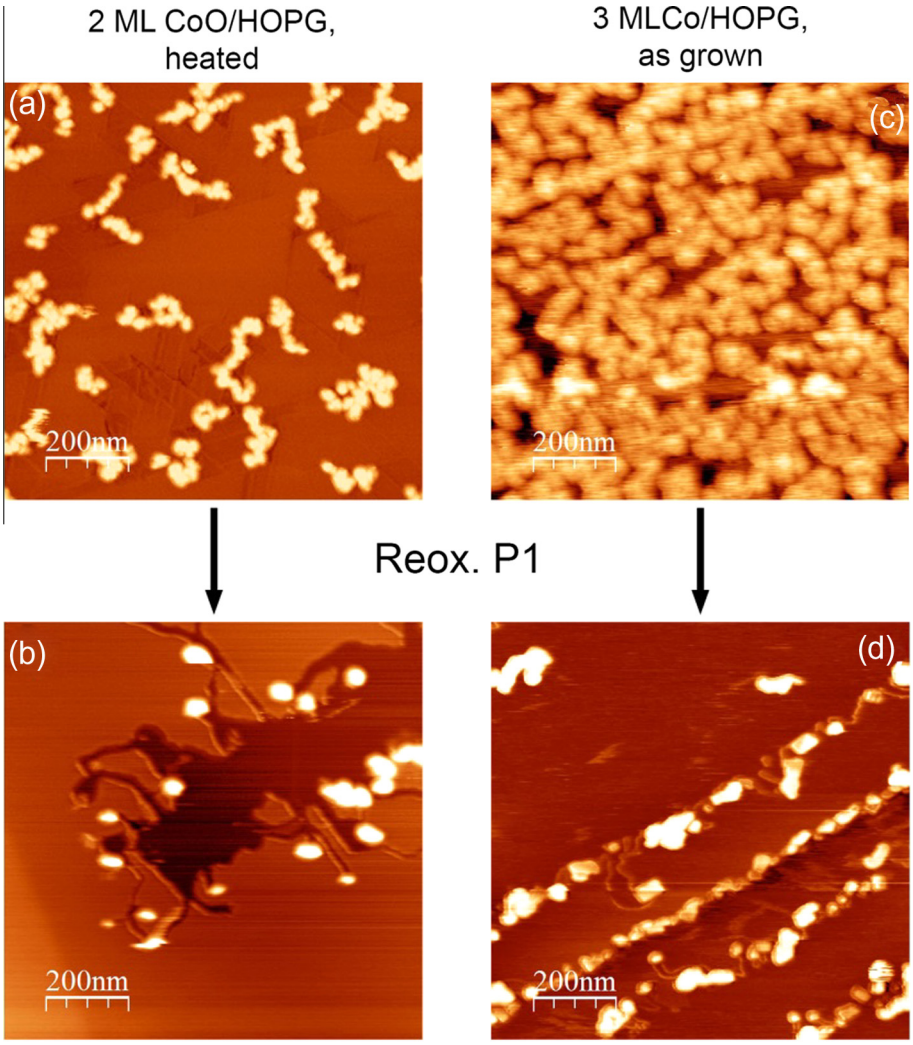

Fig. 4 – 1 × 1 μm² AFM images of (a) metallic cobalt nanoparticles as a result of the reduction of the initial CoO ultra-thin layer submitted to heating at 400 °C in UHV conditions; (b) the initial CoO ultra-thin layer submitted to the complete Reox-P1 process; (c) 3 ML of evaporated cobalt nanoparticles in UHV; (d) evaporated metallic cobalt nanoparticles submitted to the complete Reox-P1 process. (A color version of this figure can be viewed online.)

nanoparticles after the complete Reox-P1, being Co^{2+} (CoO) instead of Co_3O_4 as those of the reduced Co nanoparticles. The XPS and XAS spectra of the evaporated Co nanoparticles (labeled as grown) seem to be identical as those of the reduced Co nanoparticles shown in Fig. 1 (as heated), whose calculations clearly indicate the presence of metallic cobalt. The only difference appears in the Co 2p XPS spectra in which the binding energy for the reduced Co nanoparticles is slightly shifted by 0.17 eV towards lower binding energies (see Fig. S2 of the Supplementary information). Two possible explanations can be argued to explain this difference: different relaxation energy of the nanoparticles due to different size and different local environment of the Co atoms of the nanoparticles. The first hypothesis is not convincing since the difference in size is small (25–50 nm for the reduced nanoparticles versus 50–100 nm for the evaporated nanoparticles) and no quantum size-effects are expected in these relative large nanoparticles. Besides, the binding energy for the smallest nanoparticles should shift towards higher binding energies as relaxation energy accounts for energy losses of the photoelectrons. The most plausible hypothesis seems to be the second one, i.e. different local environment of the Co nanoparticles.

Indeed, in Fig. 6a it is shown the surface sensitive C 1s photoemission peak of clean graphite as well as for 3 ML of evaporated metallic cobalt and different coverages of CoO on HOPG. In order to make surface sensitive spectra, the inelastic mean free path of the photoelectrons has been diminished by adjusting the photon energy at 380 eV and by tilting the sample to form 60° take off angle of the photoelectrons. With these experimental conditions, the value of the inelastic mean free path of the photoelectrons is of the order of 4–6 Å, thus probing only the near surface region of the HOPG substrate. The spectra shown in Fig. 6a are dominated by the main peak of graphite located at 284.3 eV in agreement with the literature [26], however, the most important feature of this figure is that for low coverages of both, metallic Co and CoO, the graphite surface undergoes some changes,

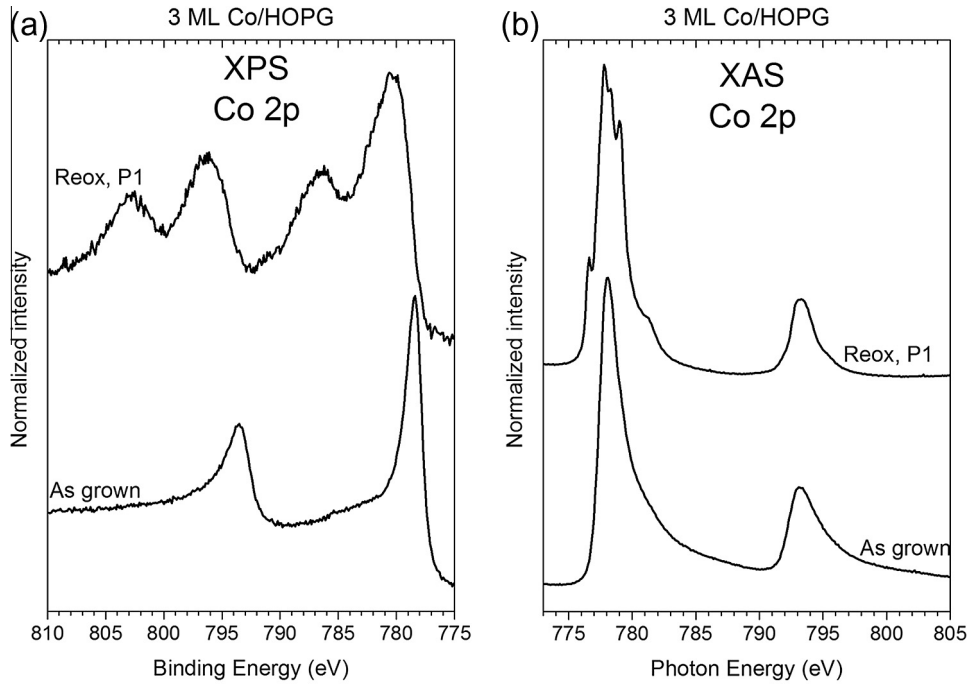

Fig. 5 – Experimental Co 2p (a) XPS and (b) XAS spectra for 3 ML of evaporated cobalt nanoparticles in UHV as grown and submitted to the complete Reox-P1 process.

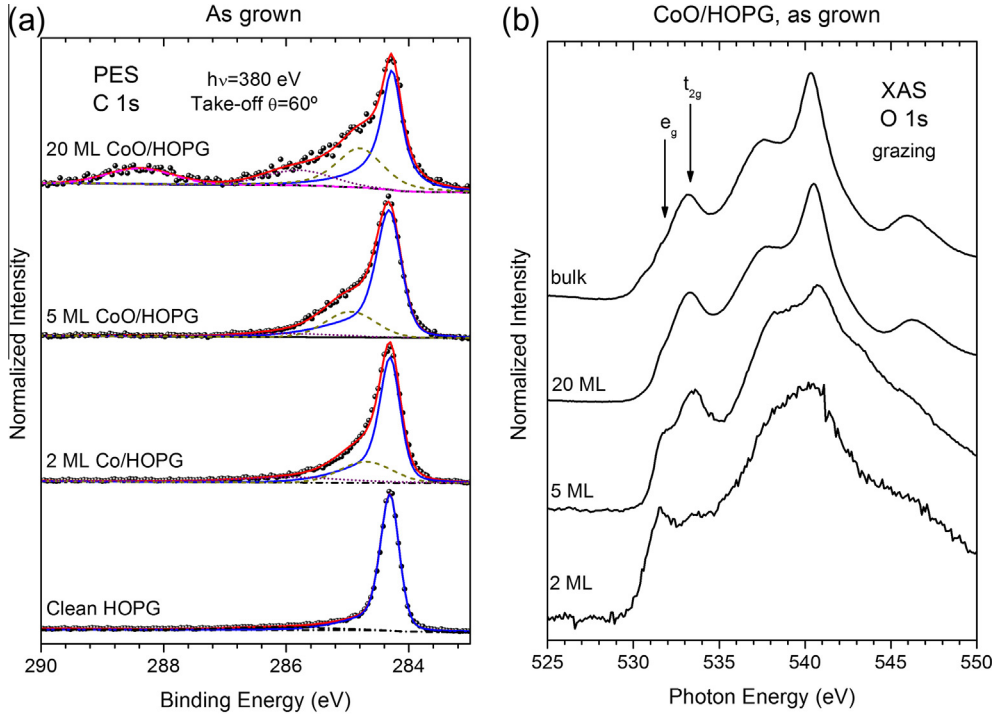

Fig. 6 – (a) Surface sensitive C 1s photoemission spectra for: clean HOPG substrate; 2 ML of evaporated cobalt in UHV; 5 ML and 20 ML of CoO as grown on HOPG (as labeled). (b) Grazing incidence O 1s XAS spectra for: 2 ML, 5 ML and 20 ML of CoO as grown on HOPG (as labeled) and bulk CoO. (A color version of this figure can be viewed online.)

appearing an extra peak located at c.a. 285 eV. This peak is commonly assigned to sp^3 bonds [27]. Thus, the appearance of this peak suggests the weakening of the sp^2 bonds in graphite by the presence of Co and CoO. However, in the case of coverages of 20 ML of CoO two more peaks appear at binding energies of about 285.8 eV and 288.5 eV. The first peak is usually assigned in the literature as due to the presence of C–O bonds and the second one is assigned to C=O bonds

[28]. These results suggest that the presence of CoO is oxidizing the HOPG surface thus weakening the sp^2 bonds of graphite. In this picture, the catalytic carbon gasification reaction of the HOPG surface is more efficient for CoO oxide grown on the surface than for metallic cobalt.

On the other hand, Fig. 6b shows the O 1s XAS spectra for different coverages of CoO as grown on HOPG taken in grazing photon incidence. In general, the O 1s XAS spectra of CoO represent the O 2p unoccupied states hybridized with the Co 3d states at threshold, thus mapping the t_{2g} and e_g sub-bands separated by crystal field. At higher energies, the spectra correspond to hybridization of O 2p with Co 4sp states. This is seen in the spectrum labeled as bulk in Fig. 6b where the t_{2g} and e_g sub-bands are clearly visible. However, in the spectrum for the early stages of growth (2 ML of CoO/HOPG), the relative intensity of these peaks is different showing a higher intensity of the e_g sub-band than in the bulk spectrum. Besides, as the spectrum of 2 ML of CoO/HOPG is taken in grazing incidence, it mainly accounts for transitions directed perpendicular to the HOPG surface. These results indicate that the O atoms at the interface are interacting with the HOPG surface or, in other words, the HOPG surface is oxidized by the presence of the cobalt oxide at the interface. These results are also consistent with the results obtained from the C 1s PES spectra shown in Fig. 6a.

3.4. *Raman study of defects on the HOPG surface*

In this section we will study the defects produced by the catalytic reaction promoted by cobalt oxides on the HOPG surface. Raman Spectroscopy is a suitable technique for the study of defects in carbon polymorphs such as carbon nanotubes, graphite and graphene [29,30]. Also the Raman spectra for cobalt oxides have been studied [31], however their intensity is too weak, especially that for CoO, due to the low polarization of the Co-O bond. As an example Fig. 7a shows the typical Raman band (G) for the clean graphite (bottom) and the carbon Raman bands for 2 ML CoO/HOPG. It is seen that the spectrum for the substrate covered by 2 ML cobalt oxide after the re-oxidation process P1 shows the typical G band for graphite and the small D band usually assigned to defects in the literature.

We have performed a combined AFM-microRaman study of the samples to relate the observed morphology of the cobalt oxides structures with the defects induced on the substrate. The images are shown in Fig. 7b where the top images correspond to AFM and those at the bottom correspond to the micro-Raman images of the same area. The Raman images resulted from mapping the different single Raman spectra collected in each pixel. These images represent the D/G bands ratio in order to have a clearer view of the defects. To compare both, Raman and AFM images we have to note that the Raman images have lower resolution than those obtained by AFM. The image taken after the Reox-P1 process shows that defects have been produced in the HOPG surface regions covered by cobalt oxide particles and their surroundings whereas the image taken after the Reox-P2 process shows only the original defects at the steps of the HOPG substrate. This confirms that the Reox-P1 process is efficient in the creation of defects in graphite and thus suitable for the creation of nanostructures on its surface, i.e. nanopatterning on the HOPG surface.

Fig. 8a shows the depth profile (XZ) micro-Raman image taken from a sample submitted to Reox-P1. This figure is a color-coded image in which the intensity of de color correlated with the Raman intensity of three different bands: the A_{1g} mode of spinel Co_3O_4 oxide (solid red cross), the D band assigned to defects in graphite (dashed blue cross) and the G band of the pure graphite substrate (dotted green cross). Fig. 8b shows the Raman spectra measured in these three

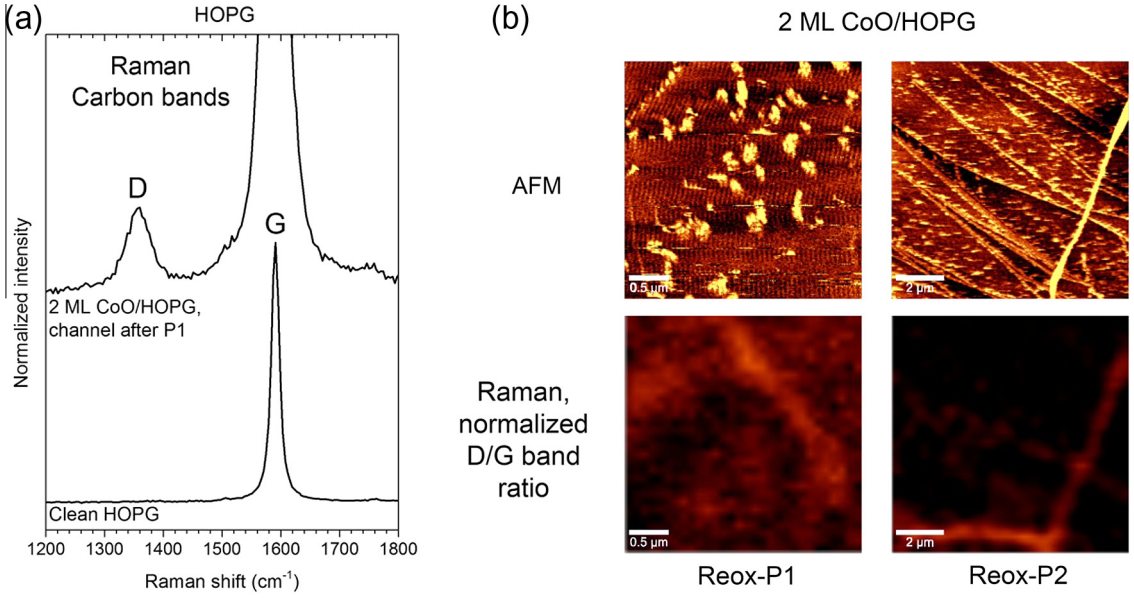

Fig. 7 – (a) Carbon Raman bands for Clean HOPG substrate (bottom) and 2 ML of CoO as grown on HOPG (top). (b) AFM (top) and micro-Raman (bottom) images of 2 ML of CoO as grown on HOPG submitted to Reox-P1 (left) and Reox-P2 (right). (A color version of this figure can be viewed online.)

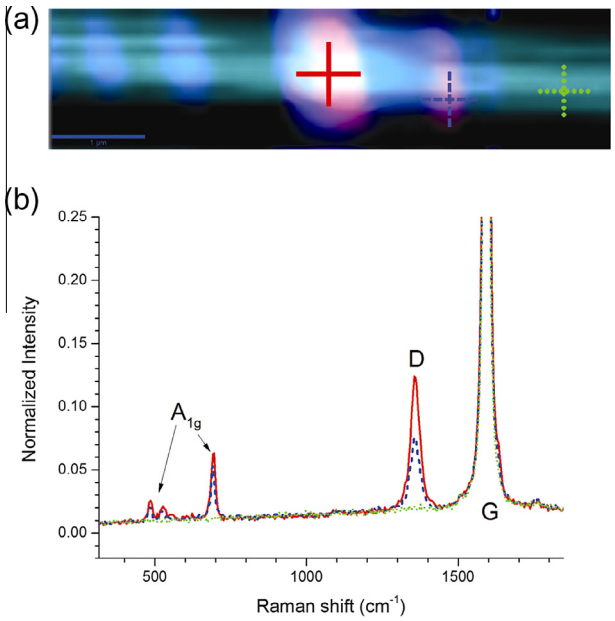

Fig. 8 – (a) Micro-Raman image of 2 ML of CoO as grown on HOPG submitted to Reox-P1. Crosses indicate the position where the bands shown at the bottom have been measured. (b) Carbon Raman bands measured as indicated at the top image. (A color version of this figure can be viewed online.)

areas, as indicated in Fig. 8a. The Raman spectra of the substrate covered by large cobalt oxide islands (solid red cross) show strong defects D band whereas the substrate uncovered (dotted green cross) shows no defects. This clearly indicates that the cobalt oxides formed upon Reox-P1 are producing a large amount of defects on the HOPG surface. There are some areas (only blue areas) in which the graphite substrate presents D band due to defects but there is not spinel Co_3O_4 oxide. These regions seem correspond to the channels displayed in AFM (Figs. 2c and 3a) at the end of which the spinel Co_3O_4 oxide is located.

4. Conclusions

In summary, we have studied an efficient method for producing nanopatterning on a HOPG surface at 400 °C using an ultrathin layer of CoO as catalyst for the carbon gasification reaction with oxygen as reactant gas. It has been demonstrated that, at these temperatures, this method is more efficient for carbon gasification than the usual method using metallic cobalt nanoparticles reported in the literature. The oxygen contained in the starting CoO layer seems to play an important role by weakening the bonds of the HOPG surface previously to the re-oxidation process. Although the first step of this process (heating at 400 °C) produce the reduction of the initial CoO layer to cobalt nanoparticles, these particles behave in a different way from those grown directly by evaporation of cobalt. This different behavior is explained by the defects created by the CoO layer on the HOPG surface previously to the re-oxidation process. The final stage of the process gives a HOPG surface with nano-channels formed by defective graphite, thus suitable for the growth of other nanostructures on this surface. The quality of the nano-channels produced by this method could be improved by controlling the amount of the initial CoO layer as well as by magnetic steering of the cobalt nanoparticles during the reaction.

Acknowledgments

This investigation has been funded by the MINECO of Spain through the CONSOLIDER CSD2008-00023, AYA2012-39832-C02-02, FIS2013-40667-P and MAT2011-26534 projects and the Comunidad de Madrid through the NANOFRONTMAG-CM P2013/MIT2850 project. Authors R.J.O.M. and M.A. thank the financial support of Conselho Nacional de Desenvolvimento Científico e Tecnológico (CNPq-Brazil). One of the authors (O.B.M.) thanks the financial support from the "Ramón y Cajal" Program of MINECO.

Appendix A. Supplementary data

Supplementary data associated with this article can be found, in the online version, at http://dx.doi.org/10.1016/j.carbon.2014.12.049.

REFERENCES

[1] Polini M, Guinea F, Lewenstein M, Manoharan HC, Pellegrini V. Artificial honeycomb lattices for electrons, atoms and photons. Nat Nanotechnol 2013;8:625. http://dx.doi.org/10.1038/nnano.2013.161.
[2] Chen Z, Lin Y, Rooks M, Avouris P. Graphene nano-ribbon electronics. Physica E 2007;40:228. http://dx.doi.org/10.1016/j.physe.2007.06.020.
[3] Pang S, Tsao HN, Feng X, Mullen K. Patterned graphene electrodes from solution-processed graphite oxide films for organic field-effect transistors. Adv Mater 2009;21:3488. http://dx.doi.org/10.1002/adma.200803812.
[4] Mühl T, Kretz J, Mönch I, Schneider CM. Parallel nanolithography in carbon layers with conductive imprint stamps. Appl Phys Lett 2000;76:786. http://dx.doi.org/10.1063/1.125895.
[5] Eagle SC, Fedder GK. Writing nanometer-scale pits in sputtered carbon films using the scanning tunneling microscope. Appl Phys Lett 1999;74:3902. http://dx.doi.org/10.1063/1.124218.
[6] Ci L, Xu Z, Wang L, Gao W, Ding F, Kelly KF, et al. Controlled nanocutting of graphene. Nano Res 2008;1:116. http://dx.doi.org/10.1007/s12274-008-8020-9.
[7] Severin N, Kirstein S, Sokolov IM, Rabe JP. Rapid trench channeling of graphenes with catalytic silver nanoparticles. Nano Lett 2009;9:457. http://dx.doi.org/10.1021/nl8034509.
[8] Konishi S, Sugimoto W, Murakami Y, Takasu Y. Catalytic creation of channels in the surface layers of highly oriented pyrolytic graphite by cobalt nanoparticles. Carbon 2006;44:2338. http://dx.doi.org/10.1016/j.carbon.2006.05.003.
[9] Datta SS, Strachan DR, Khamis SM, Johnson ATC. Crystallographic etching of few-layer graphene. Nano Lett 1912;2008:8. http://dx.doi.org/10.1021/nl080583r.
[10] Bulut L, Hurt RH. A magneto-catalytic writing technique for etching complex channel patterns into graphenic carbons. Adv Mater 2010;22:337. http://dx.doi.org/10.1002/adma.200901932.

[11] Keep C, Terry S, Wells M. Studies of the nickel-catalyzed hydrogenation of graphite. J Catal 1980;66:451. http://dx.doi.org/10.1016/0021- 517(80)90047-0.
[12] McKee DW. Metal oxides as catalysts for the oxidation of graphite. Carbon 1970;8:623. http://dx.doi.org/10.1016/0008-6223(70)90055-2.
[13] Kim Do-Hyun, Waki Keiko. Crystal defects on multi-walled carbon nanotubes by cobalt oxide. J Nanosci Nanotechnol 2010;10:2375. http://dx.doi.org/10.1166/jnn.2010.1911.
[14] Oktaviano HS, Yamada K, Waki K. Nano-drilled multiwalled carbon nanotubes: characterizations and application for LIB anode materials. J Mater Chem 2012;22:25167. http://dx.doi.org/10.1039/C2JM34684B.
[15] Lee Sang Yun, Kim Do-Hyun, Choi Seung Chol, Lee Dong-Jin, Choi Ji Yoon, Kim Hong-Dae. Porous multi-walled carbon nanotubes by using catalytic oxidation via transition metal oxide. Microporous Mesoporous Mater 2014;194:46. http://dx.doi.org/10.1016/j.micromeso.2014.03.040.
[16] Díaz-Fernández D, Méndez J, Bomatí-Miguel O, Yubero F, Mossanek RJO, Abbate M, et al. The growth of cobalt oxides on HOPG and SiO_2 surfaces: a comparative study. Surf Sci 2014;624:145. http://dx.doi.org/10.1016/j.susc.2014.02.007.
[17] Ohring M. In: Materials science of thin films: deposition and structure. San Diego: Academic Press; 2002. p. 608 [chapter 10].
[18] Abbate M, Goedkoop JB, de Groot FMF, Grioni M, Fuggle JC, Hofmann S, et al. Probing depth of soft X-ray absorption spectroscopy measured in total-electron-yield mode. Surf Interface Anal 1992;18:65. http://dx.doi.org/10.1002/sia.740180111.
[19] Díaz J, Paolicelli G, Ferrer S, Comin F. Separation of the sp^3 and sp^2 components in the C1 s photoemission spectra of amorphous carbon films. Phys Rev B 1996;54:8064. http://dx.doi.org/10.1103/PhysRevB.54.8064.
[20] Martinez L, Tello M, Díaz M, Román E, García R, Huttel Y. Aspect-ratio and lateral-resolution enhancement in force microscopy by attaching nanoclusters generated by an ion cluster source at the end of a silicon tip. Rev Sci Instrum 2011;82:023710. http://dx.doi.org/10.1063/1.3556788.
[21] Horcas I, Fernández R, Gómez Rodríguez JM, Colchero J, Gómez Herrero J, Baró AM. WSXM: a software for scanning probe microscopy and a tool for nanotechnology. Rev Sci Instrum 2007;78:013705. http://dx.doi.org/10.1063/1.2432410.
[22] Zafeiratos S, Dintzer T, Teschner D, Blume R, Hävecker M, Knop-Gericke A, et al. Methanol oxidation over model cobalt catalysts: influence of the cobalt oxidation state on the reactivity. J Catal 2010;269:309. http://dx.doi.org/10.1016/j.jcat.2009.11.013.
[23] de Groot FMF, Abbate M, van Elp J, Sawatzky GA, Ma YJ, Chen CT, et al. Oxygen 1s and cobalt 2p X-ray absorption of cobalt oxides. J Phys: Condens Matter 1993;5:2277. http://dx.doi.org/10.1088/0953-8984/5/14/023.
[24] Pisula W, Nliangfeng X, Müllen K. Self-organization of nanographenes. In: Carbon nanotubes and related structures. Wiley-VCH Verlag GmbH & Co. KGaA; 2010. p. 405–53 [ch14, DOI: 10.1002/9783527629930].
[25] García Ricardo. Amplitude modulation atomic force microscopy. New York: Ed. Wiley; 2010 [ISBN: 978-3-527-40834-4].
[26] Webb MJ, Palmgren P, Pal P, Karis O, Grennberg H. A simple method to produce almost perfect graphene on highly oriented pyrolytic graphite". Carbon 2011;49:3242. http://dx.doi.org/10.1016/j.carbon.2011.03.050.
[27] Rousseau B, Estrade-Szwarckopf H, Thoman A-L, Brault P. Stable C-atom displacements on HOPG surface under plasma low-energy argon-ion bombardment. Appl Phys A 2003;77:591. http://dx.doi.org/10.1007/s00339-002-1538-x.
[28] Miller DJ, Biesinger MC, Mcintyre NS. Interactions of CO_2 and CO at fractional atmosphere pressures with iron and iron oxide surfaces: one possible mechanism for surface contamination? Surf Interface Anal 2002;33:299. http://dx.doi.org/10.1002/sia.1188.
[29] Dresselhaus MS, Jorio A, Souza Filho AG, Saito R. Defect characterization in graphene and carbon nanotubes using Raman spectroscopy. Philos Trans R Soc London A 2010;368:5355. DOI : 0.1098/rsta.2010.0213.
[30] Malard LM, Pimenta MA, Dresselhaus G, Dresselhaus MS. Raman spectroscopy in graphene. Phys Rep 2009;473:51. http://dx.doi.org/10.1016/j.physrep.2009.02.003.
[31] Gallant D, Pézolet M, Simard S. Optical and physical properties of cobalt oxide films electrogenerated in bicarbonate aqueous media. J Phys Chem B 2006;110:6871. http://dx.doi.org/10.1021/jp056689h.